Journal of Virology®

VIRUS-CELL INTERACTIONS

Measles Virus Bearing Measles Inclusion Body Encephalitis-Derived Fusion Protein Is Pathogenic after Infection via the Respiratory Route

Cyrille Mathieu,[a,b,c] Marion Ferren,[a,b,c] Eric Jurgens,[a,b] Claire Dumont,[c] Ksenia Rybkina,[a,b] Olivia Harder,[d] Debora Stelitano,[a,b] Silvia Madeddu,[a,b,e] Giuseppina Sanna,[a,b,e] Dayna Schwartz,[a,b] Sudipta Biswas,[a,b] Diana Hardie,[f] Takao Hashiguchi,[g] Anne Moscona,[a,b,h,i] Branka Horvat,[c] Stefan Niewiesk,[d] Matteo Porotto[a,b,j]

[a]Center for Host-Pathogen Interaction, Columbia University Medical Center, New York, New York, USA
[b]Department of Pediatrics, Columbia University Medical Center, New York, New York, USA
[c]CIRI, International Center for Infectiology Research, Inserm, U1111, University Claude Bernard Lyon 1, CNRS, UMR5308, Ecole Normale Supérieure de Lyon, Lyon, France
[d]Department of Veterinary Biosciences, College of Veterinary Medicine, The Ohio State University, Columbus, Ohio, USA
[e]Department of Biomedical Sciences, University of Cagliari, Cittadella Universitaria, Monserrato, Cagliari, Italy
[f]Division of Medical Virology, Department of Clinical Laboratory Sciences, University of Cape Town and National Health Laboratory Service, Cape Town, South Africa
[g]Department of Virology, Faculty of Medicine, Kyushu University, Fukuoka, Japan
[h]Department of Microbiology and Immunology, Columbia University Medical Center, New York, New York, USA
[i]Department of Physiology and Cellular Biophysics, Columbia University Medical Center, New York, New York, USA
[j]Department of Experimental Medicine, University of Study of Campania Luigi Vanvitelli, Naples, Italy

ABSTRACT A clinical isolate of measles virus (MeV) bearing a single amino acid alteration in the viral fusion protein (F; L454W) was previously identified in two patients with lethal sequelae of MeV central nervous system (CNS) infection. The mutation dysregulated the viral fusion machinery so that the mutated F protein mediated cell fusion in the absence of known MeV cellular receptors. While this virus could feasibly have arisen via intrahost evolution of the wild-type (wt) virus, it was recently shown that the same mutation emerged under the selective pressure of small-molecule antiviral treatment. Under these conditions, a potentially neuropathogenic variant emerged outside the CNS. While CNS adaptation of MeV was thought to generate viruses that are less fit for interhost spread, we show that two animal models can be readily infected with CNS-adapted MeV via the respiratory route. Despite bearing a fusion protein that is less stable at 37°C than the wt MeV F, this virus infects and replicates in cotton rat lung tissue more efficiently than the wt virus and is lethal in a suckling mouse model of MeV encephalitis even with a lower inoculum. Thus, either during lethal MeV CNS infection or during antiviral treatment *in vitro*, neuropathogenic MeV can emerge, can infect new hosts via the respiratory route, and is more pathogenic (at least in these animal models) than wt MeV.

IMPORTANCE Measles virus (MeV) infection can be severe in immunocompromised individuals and lead to complications, including measles inclusion body encephalitis (MIBE). In some cases, MeV persistence and subacute sclerosing panencephalitis (SSPE) occur even in the face of an intact immune response. While they are relatively rare complications of MeV infection, MIBE and SSPE are lethal. This work addresses the hypothesis that despite a dysregulated viral fusion complex, central nervous system (CNS)-adapted measles virus can spread outside the CNS within an infected host.

KEYWORDS central nervous system infections, *in vivo* infection, pathogenesis, viral fusion

Citation Mathieu C, Ferren M, Jurgens E, Dumont C, Rybkina K, Harder O, Stelitano D, Madeddu S, Sanna G, Schwartz D, Biswas S, Hardie D, Hashiguchi T, Moscona A, Horvat B, Niewiesk S, Porotto M. 2019. Measles virus bearing measles inclusion body encephalitis-derived fusion protein is pathogenic after infection via the respiratory route. J Virol 93:e01862-18. https://doi.org/10.1128/JVI.01862-18.

Editor Rebecca Ellis Dutch, University of Kentucky College of Medicine

Address correspondence to Cyrille Mathieu, cyrille.mathieu@inserm.fr, or Matteo Porotto, mp3509@cumc.columbia.edu.

Received 29 October 2018
Accepted 30 January 2019
Accepted manuscript posted online 6 February 2019
Published 3 April 2019

Despite the availability of a measles virus (MeV) vaccine and ongoing efforts by the Measles Initiative to increase vaccine coverage, MeV has not been eradicated and has caused 100,000 to 140,000 deaths globally every year since 2010 (1–3). MeV eradication by vaccination is complicated by several biological and societal factors, including incomplete protection in the presence of maternal antibodies (4) and decreasing vaccination rates, often related to parental concerns over safety (5). These factors contribute to the recent resurgence of MeV infection in Europe and the United States (6).

MeV initially infects activated SLAM/CD150-expressing immune cells in the respiratory tract and thereby enters the lymphatic circulation (7). Viral replication occurs in SLAM/CD150-expressing lymphocytes in draining lymph nodes and is followed by viremia. Late in infection, MeV infects respiratory epithelial cells after attaching to nectin-4 expressed on the basolateral membranes of these cells and exits the host for interhost transmission from the respiratory tract (8, 9).

Cellular infection by MeV starts with attachment to cell surface receptors, followed by entry that is mediated by fusion between the viral and host membranes. Both initial steps rely on the concerted actions of the MeV receptor binding (H) and fusion (F) surface glycoproteins, which together make up the viral fusion complex (10, 11). F is synthesized as a precursor (F_0) that is cleaved within the infected cell prior to egress to yield the prefusion F, which exists as a homotrimer composed of three C-terminal F_1 subunits associated via disulfide bonds with three N-terminal F_2 subunits. The newly produced viral particles bear the trimeric F structure kinetically trapped in a metastable conformation on the surface of the viral membrane (12). In this metastable conformation, F can be activated to mediate fusion when the H glycoprotein engages a target cell surface entry receptor (SLAM/CD150 or nectin-4 for wild-type [wt] strains) (7–9). Upon receptor engagement, H triggers the prefusion F protein to undergo a conformational change, extending to expose the hydrophobic fusion peptide that inserts into the host cell membrane. Following insertion, F refolds into a stable postfusion 6-helix bundle structure, bringing the viral and target cell membranes together to initiate the formation of the fusion pore. The propensity of F to refold to the postfusion state relies on the interaction between two complementary heptad repeat (HR) regions at the N and C termini of the protein (HRN and HRC, respectively). This step of fusion can be inhibited by peptides corresponding to these HR regions (13).

Days to years after the acute phase of infection, central nervous system (CNS) MeV infection can lead to fatal complications (14–16). Subacute sclerosing panencephalitis (SSPE) develops in a small percentage of immune-competent patients several years after initial infection. SSPE is characterized by persistent infection of the brain and hypermutated MeV genomic RNA and viral transcripts, as well as defective viral particle assembly (17–19). Measles inclusion body encephalitis (MIBE) occurs in immunocompromised patients days to months after infection or vaccination with the live-attenuated MeV vaccine (15, 20, 21) and has been suggested to be associated with hyperfusogenic viral fusion complexes that can mediate viral entry in the absence of known MeV receptors (22, 23). Mechanisms governing MeV infection and spread in the CNS remain poorly understood, although CNS invasion seems to require the F protein and thus may feasibly be targeted by fusion inhibitors (12, 24–26).

MeV CNS infection by viruses bearing F proteins mutated in the HRC domain has been observed (22, 23, 27, 28), but growth of these viruses outside the CNS was thought to be impaired (29). Viral isolates from two patients with fatal MIBE contained F with an L454W mutation (22) that increased the thermal lability of the F protein in its metastable state. We previously showed that the L454W mutation in F affects cell entry and that recombinant MeV IC323-F L454W expressing green fluorescent protein spread in cells that lack a known MeV receptor. In cell-cell fusion assays, transfection with L454W F alone mediates fusion independently of the H protein (23). This is in distinction to other hyperfusogenic MeV isolates that depend on H for membrane fusion (30).

Virus bearing L454W F that was isolated from patients could either have arisen *de novo* in the CNS or have been present in the circulating wild-type viral population;

either way, this mutation appears to have undergone positive selection in the CNS. The virus's origin could not be determined. A recent report showed that a virus bearing L454W F emerges under the selective pressure of certain small-molecule fusion inhibitors, including fusion inhibitory peptide (FIP) (31). These findings raised the question of whether a virus bearing this neuropathogenic F protein can be found outside the CNS and spread within an individual. To address this question, we assessed the L454W F variant virus *in vivo*, using an engineered virus expressing enhanced green fluorescent protein (EGFP) with the mutated F on the background of the IC323 wt MeV strain (MeV IC323-EGFP-F L454W) and an identical control engineered virus bearing wt F. In cotton rat lungs, MeV IC323-EGFP-F L454W replicates better than the wt virus. The lethal dose for MeV IC323-EGFP-F L454W virus in a suckling transgenic mouse model is significantly lower than for wt virus but similar to the wt virus, and infection can be blocked by fusion inhibitory peptides. The F L454W mutation thus enhances viral growth in cotton rat lung tissue and correlates with increased pathogenicity in mice. We pursued the striking finding that this neuropathogenic MeV with a dysregulated fusion complex is pathogenic outside the CNS and can infect two animal models by the respiratory route.

RESULTS

F glycoproteins from neuropathogenic measles viruses. We and others have previously described several mutations in the MeV F glycoprotein (L454W, T461I, and N462K) in neuropathogenic MeV strains either isolated from patients or generated in laboratory settings (22, 23, 28). These mutations were associated with decreased thermal stability of the prefusion metastable state of the F protein. We mapped these mutations onto structures of the prefusion (MeV F; PDB identifier [ID] 5YXW [12]) and postfusion (modeled on HPIV3 F; PDB ID 1ZTM [32]) conformations of MeV F (Fig. 1). The three mutated residues (L454W, T461I, and N462K) were all located within the C-terminal heptad repeat domain (HRC). In the prefusion structure, the L454W mutation causes steric hindrance within the same protomer. The T461I and N462K mutations map in an α-helical region of the HRC domain. These three mutations occur at the portion of the HRC domain where the head and stalk regions of the prefusion conformation meet. Interactions at this junction are likely to be important for stabilizing the prefusion state, and consequently, mutations in this region would lead to decreased stability of the MeV F prefusion structure, as our data have previously suggested (23).

Thermal stability and fusion inhibitor susceptibility of neuropathogenic MeV variants. Hyperfusogenic variants of MeV F mutated in the HRC domain are less thermostable than viruses with the wild-type F protein (23). To determine whether viruses bearing the mutated F proteins are less stable than wt virus, thermal inactivation profiles were obtained (Fig. 2). Viruses ($\sim$1,000 PFU in 100 μl) were incubated at various temperatures (from 4 to 55°C for the times indicated in Fig. 2). The viral titers were not affected by 30 min at 4°C. At 37°C, the infectivity of only the F-L454W and F-N462K variants decreased significantly (to 50% and 12%, respectively). This decrease correlates with the lower thermal stability of these F proteins (23). Thirty minutes at 45°C abrogated the infectivity of the three mutant viruses by more than 90% compared to that of the wt, which retained more than 40% of its original viral titer ($P < 0.001$, two-way analysis of variance [ANOVA] with Bonferroni's posttest). After 10 min at 50°C, only the wt virus was still infectious, becoming noninfectious only after 10 min at 55°C. These results confirm that the infectivity of recombinant viruses harboring the hyperfusogenic mutated F HRC correlates with the lower thermal stability of their respective fusion proteins (23).

HRC4 fusion inhibitory peptide inhibits fusion and spread by the CNS-adapted variants. We have shown that a dimeric cholesterol-conjugated fusion inhibitory peptide (HRC4) blocks infection with wt MeV (G954, WTFb, and IC323 strains) *in vitro*, *ex vivo*, and *in vivo* in cotton rats and mice (33, 34). Here, fusion inhibition by HRC4 was assessed in an *in vitro* cell-cell fusion assay using 293T cell targets expressing either of the two known MeV receptors (CD150/SLAM and nectin-4) (Fig. 3). We have noted

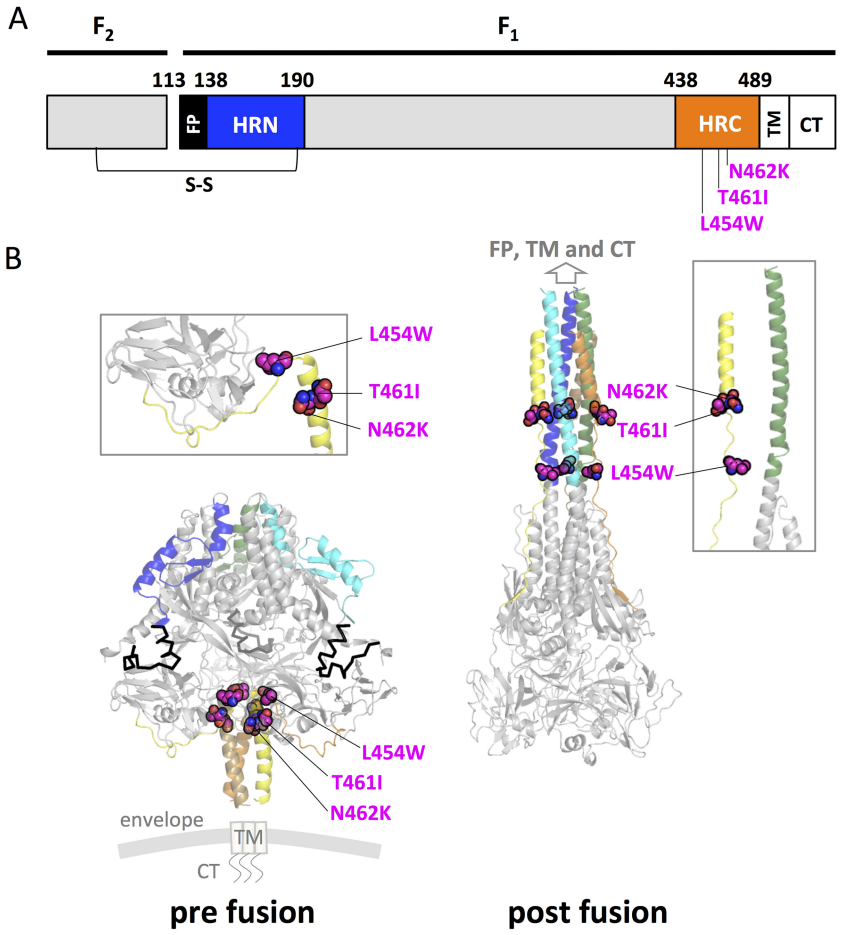

FIG 1 Location of substitutions within the F protein from CNS-adapted virus. (A) Schematic of MeV F fusion peptide (FP) with N-terminal heptad repeat (HRN), C-terminal heptad repeat (HRC), transmembrane (TM), and cytoplasmic (CT) domains indicated. (B) Ribbon diagrams representing a crystal structure of the prefusion conformation of MeV F (left, PDB 5YXW) and a model of a postfusion conformation of F (right, based on the postfusion HPIV3 F; PDB 1ZTM). The HRN (blue, green, and cyan) and the HRC (orange, brown, and yellow) domains are identified. Three substitutions (L454W, T461I, and N462K) in the HRC domain in neuropathogenic strains that side residues of the indicated amino acid position are represented as a sphere model. Color coding of substitutions: magenta, carbon; blue, nitrogen; and red, oxygen.

this assay to be the most stringent *in vitro* quantitative measure of viral inhibition. For these experiments, a small-molecule fusion protein inhibitor, *N*-(3-cyanophenyl)-2-phenylacetamide (3G) was assessed in parallel with HRC4. In contrast to the HRC-derived peptides, which block fusion after F activation, 3G stabilizes the prefusion state of the F protein (35, 36). The latter mechanism of action is shared by a previously described fusion inhibitory peptide (FIP; carbobenzoxy [Z]-D-Phe-Phe-Gly), an inhibitor that elicited resistant viruses, including one bearing an L454W F (31); therefore, we expected the L454W to be resistant to 3G.

Effector cells transfected with H and either wt F or F L454W were allowed to fuse with target cells expressing CD150/SLAM, nectin-4, or no known receptor (mock transfected) in the presence of the HRC4 or 3G fusion inhibitors. After 24 h, fusion was evaluated using beta-galactosidase complementation (37). The 50% inhibitory concentration (IC_{50}) of HRC4 for MeV F wt was between 10 and 50 nM in the presence of the SLAM/CD150 or nectin-4. The IC_{50} of HRC4 for MeV F L454W was below 0.2 nM in the presence of the SLAM/CD150 or nectin-4 transfected cells, while in the presence of mock-transfected target cells, we observed almost 100% inhibition even at the lowest concentration tested (0.2 nM). Note that wt F did not mediate fusion with mock-

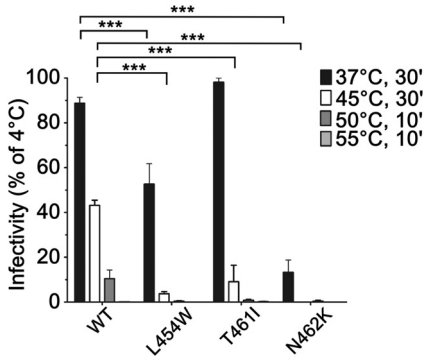

FIG 2 Thermal stability of MeV IC323 viruses bearing wild-type and mutant F proteins. Viruses bearing the indicated F proteins (*x* axis) were incubated at the indicated temperatures and times. The *y* axis represents the percentage infectivity (on Vero SLAM) compared to viruses incubated at 4°C. Results are expressed as means ± standard deviations from 3 separate experiments performed in triplicates. ***, $P < 0.001$ by two-way ANOVA with Bonferroni's posttest.

transfected cells. The IC_{50} of 3G for MeV F wt was around 10,000 to 20,000 nM in the presence of the SLAM/CD150 or nectin-4. With 3G for MeV F L454W in the presence of the SLAM/CD150 or nectin-4 transfected cells, the IC_{50} was reached only at the highest concentration used (100,000 nM). The IC_{50} dropped in the presence of mock-transfected target cells to ~50,000 nM. Thus, susceptibility to HRC-derived fusion inhibitors was higher for the F L454W than for the wt F. For 3G, we confirmed the previous findings that the L454W mutation in F confers resistance to this fusion inhibitor (12, 31, 35, 36).

The antiviral activity of HRC4 and 3G was next assessed against MeV IC323-EGFP-F L454W live virus infection (Fig. 4). Since the virus bearing L454W F spreads in the absence of a known MeV entry receptor (23), we compared the inhibitory efficacies in Vero cells expressing SLAM/CD150 (Vero-SLAM) and Vero cells that express no known MeV receptor (Fig. 4). After a 90-min infection with either wt IC323-EGFP or IC323-EGFP-F L454W viruses, cells were treated with the compounds and visualized at several time points (24, 48, and 72 h). Without treatment, the two viruses spread and formed large syncytia after 48 h in Vero-SLAM cells. In Vero cells (without receptor), MeV wt did not spread, while MeV IC323-EGFP-F L454W formed syncytia that were smaller than those formed in the presence of CD150/SLAM. The 3G posttreatment at 2,000 nM resulted in a reduction of syncytium size formed by wt MeV in Vero-SLAM cells but had no significant effect on the F L454W mutant in either cell type. HRC4 peptide treatment blocked both viruses in the presence or absence of receptor. The finding that HRC4 but not 3G inhibits MeV IC323-EGFP-F L454W suggests that HRC4 minimizes viral spread by inhibiting activated F from proceeding to fusion. Additional data are shown in Fig. S1 in the supplemental material.

Pathogenesis and protection against lethal infection with MeV IC323-EGFP-F L454W *in vivo*. Growth of MeV IC323-EGFP-F L454W in lung tissue was assessed in cotton rats (Fig. 5A). Cotton rats were infected intranasally with 10^5 50% tissue culture infective dose ($TCID_{50}$) of recombinant MeV IC323 bearing the wt F or the mutated L454W F. Four days postinfection, the animals were sacrificed and the lung viral titers were assessed. There were significantly more infectious particles in the lungs of animals infected with the hyperfusogenic mutant (L454W F) than in those infected with the wt virus ($P < 0.001$, Mann-Whitney U test).

As a complementary infection model, we assessed wt MeV IC323-EGFP and MeV IC323-EGFP-F L454W infection in a SLAM transgenic suckling mouse model of MeV lethal encephalitis that we have previously used for wt MeV infection (33) (Fig. 5B). Suckling mice were infected intranasally with either 5,000 or 10,000 PFU of wt MeV IC323-EGFP. Half of the animals died with the lowest dose (4 of 8) and only 1 of 7 animals survived the highest viral dose, suggesting that 5,000 PFU was approximately

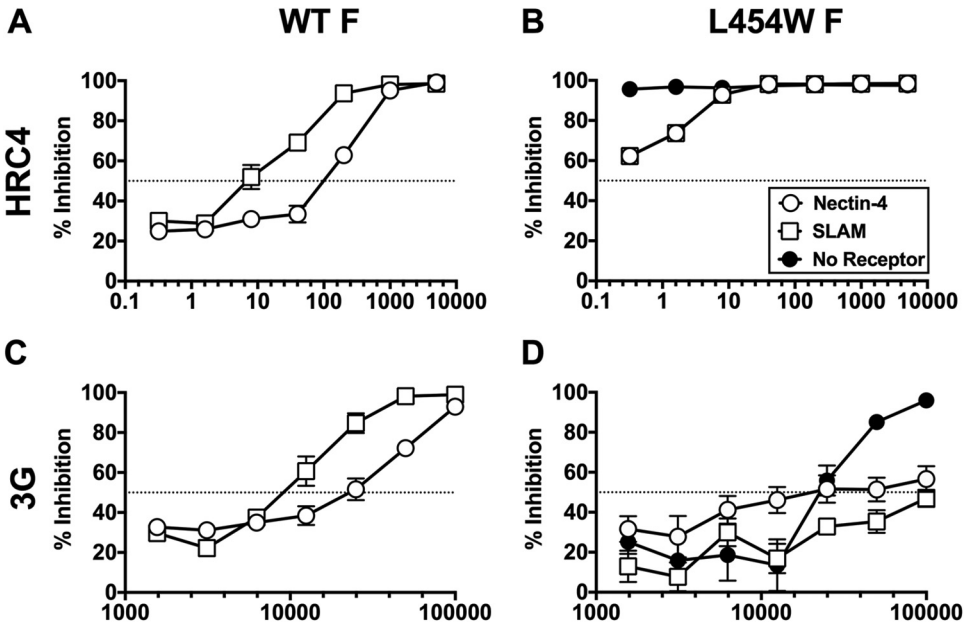

FIG 3 Inhibition of cell fusion of cells transiently expressing MeV F and MeV receptors. HEK 293T cells were cotransfected with either MeV IC323-WT F (A, C) or MeV IC323-F L454W (B, D), α-subunit of β-galactosidase, and wt IC323 MeV H. Transfected cells were subsequently overlaid 3 h posttransfection with HEK 293T cells expressing the indicated receptors (nectin-4, SLAM/CD150, or no receptor; only for F L454W, since wt F does not mediate fusion in the absence of receptor) and the ω-subunit of β-galactosidase in the presence of decreasing concentrations of HRC4 (A, B) or 3G (C, D). Cells were then incubated overnight to permit fusion. Resulting luminescence from β-galactosidase activity was quantified using Tecan Infinite M1000 Pro. Results depict means and standard errors of the means (SEMs) from two (3G) or three (HRC4) biological replicates of three technical replicates each. Dotted lines indicate 50% inhibition.

the 50% lethal dose (LD_{50}) for the wt virus. Suckling mice were infected with 500 PFU of the MeV IC323-EGFP-F L454W variant (Fig. 5C). This dose led to 80% lethality within 12 days, suggesting that this dose was above the LD_{50}. To better understand whether F L454W mutation would confer the ability to MeV to propagate faster *in vivo*, we intranasally coinfected SLAM transgenic suckling animals with 1,000 PFU of both MeV IC323-tdTomato-F wt and the MeV IC323-EGFP-F L454W variant. After 4 days, we only detected EGFP (by immune staining) in lungs, in meninges, and in neural cells in brain parenchyma (i.e., ventricle, cortex, and cerebellum areas) in all animals (Fig. 5D to G). Infection with MeV IC323-tdTomato-F wt was not detected after 4 days, a result that is consistent with the late infection observed with other wt MeV (38) These results suggest that virus bearing the F L454W mutation infects better and spreads more efficiently in both lung and CNS than the wt in this animal model.

Intranasal administration of HRC4 fusion inhibitory peptides protected SLAM transgenic suckling mice from fatal CNS infection with wt MeV (33). To evaluate the efficacy of HRC4 prophylaxis against MeV IC323-EGFP-F L454W *in vivo*, an infection was performed with 5,000 PFU of virus either with or without intranasal administration of HRC4 peptide 24 h before and 4 h after infection (33) (Fig. 6). Although 5,000 PFU infection was 100% lethal for untreated mice between day 7 and day 14 after infection, all infected animals that were treated with HRC4 24 h before and 4 h after infection survived. Thus, the pretreatment with HRC4 resulted in 100% survival ($P < 0.0001$, Mantel-Cox test) despite the very high viral inoculum, and the treated animals had no clinical manifestations.

DISCUSSION

Central nervous system (CNS) complications may occur soon after acute MeV infection in the case of acute encephalomyelitis or years after infection, as a result of viral persistence in SSPE. SSPE has recently been noted to be more common than

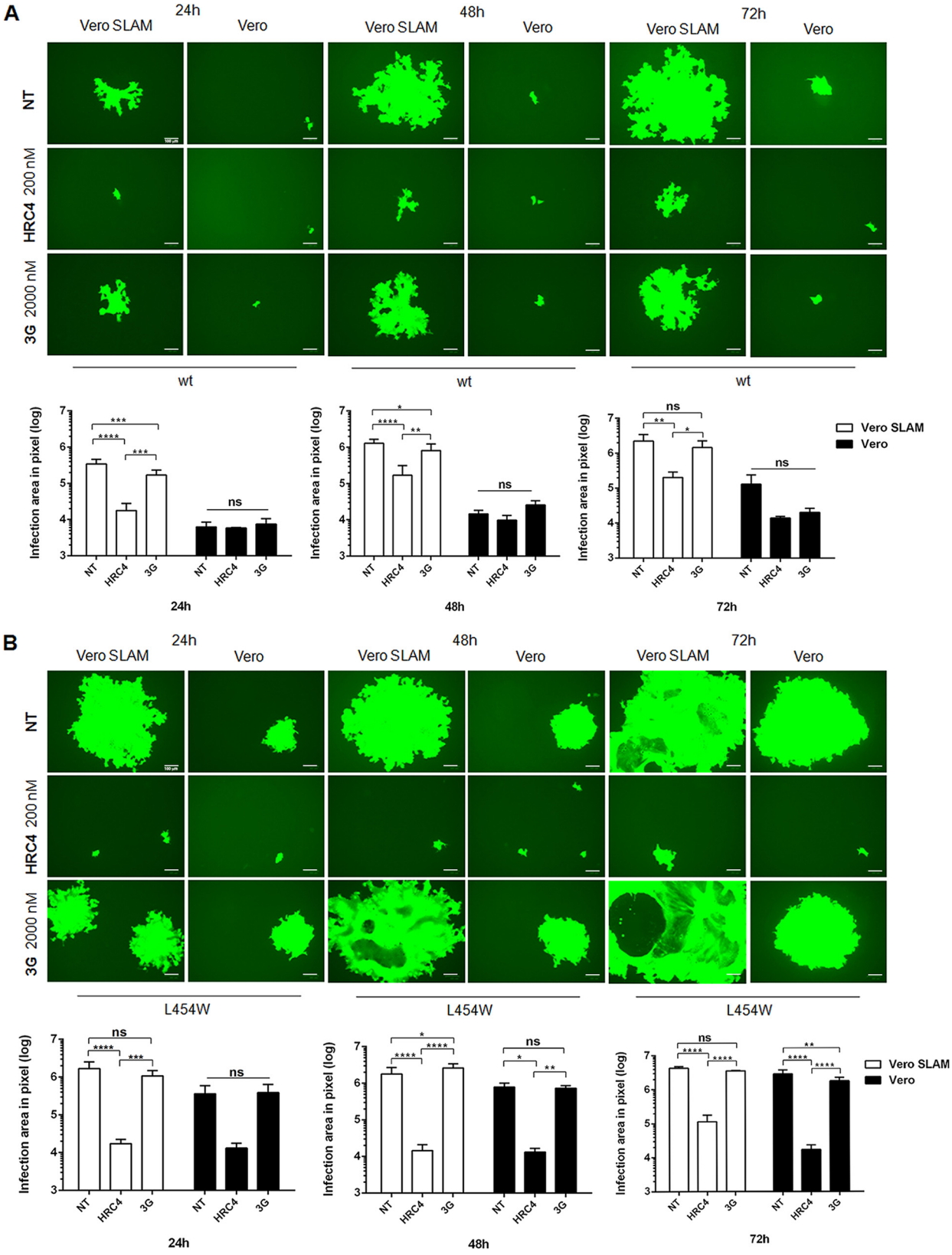

FIG 4 Inhibition of viral spread. Effect of fusion inhibitors on the areas of plaques formed by the MeV wt (A) and CNS-adapted variant virus bearing the L454W F (B) in infected Vero or Vero SLAM cells. The indicated fusion inhibitors were added after the 120-min adsorption period. Pictures were taken 24, 48, and 72 h postinfection using a ZOE Fluorescent cell imager (Bio-Rad) (bars, 100 μm). Areas of infection in pixels were measured using ImageJ software on images randomly acquired from separate experiments. ns, not significant; *, $P < 0.05$; **, $P < 0.01$; ***, $P < 0.001$; ****, $P < 0.0001$ (two-way ANOVA, $n = 3$ at least).

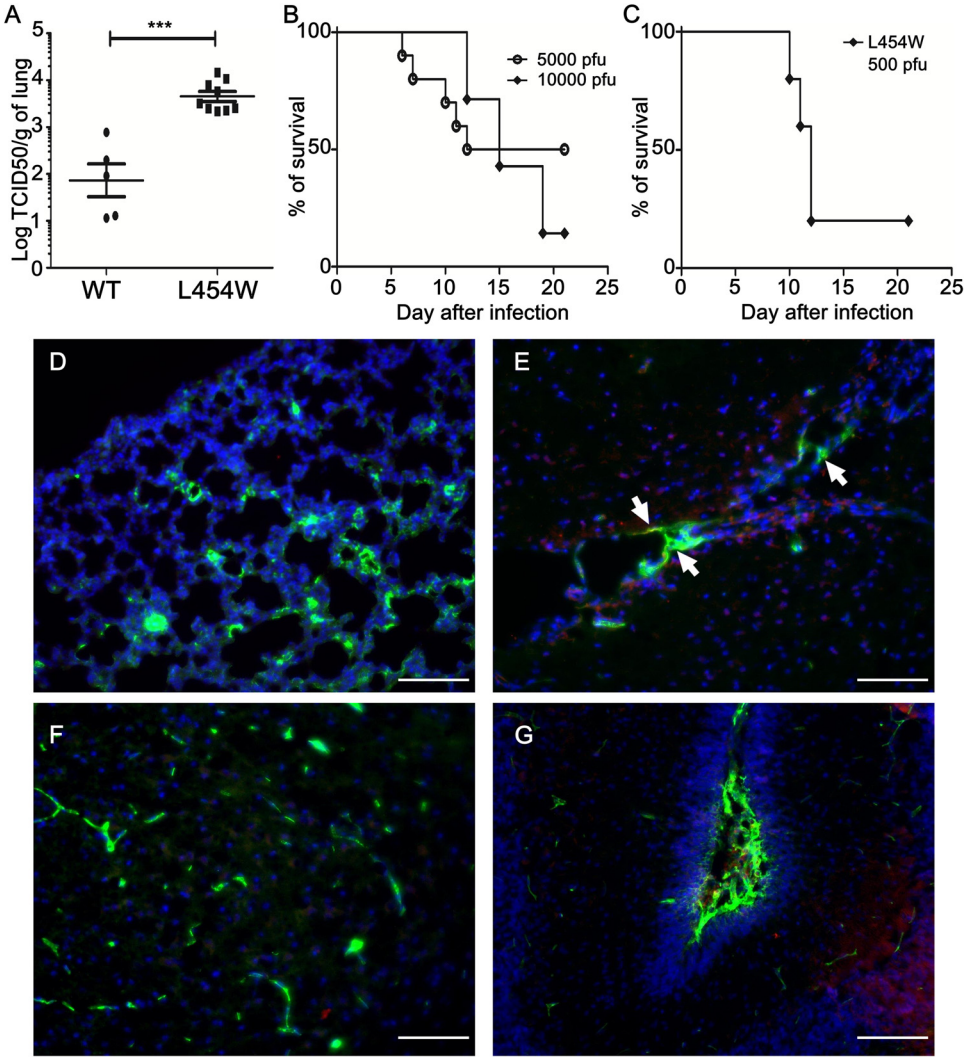

FIG 5 *In vivo* infection with virus bearing the L454W F. (A) Cotton rats ($n = 8$) were infected intranasally with MeV IC323-EGFP and MeV IC323-EGFP F L454W F viruses and were euthanized at 4 days postinfection. MeV titration of lung homogenates showed that L454W F bearing virus grew to a significantly higher titer than wt virus in cotton rats ($P = 0.001$ by the Mann-Whitney U test). The limit of viral detection was 10^2 median tissue culture infective dose per gram of tissue ($TCID_{50}$/g). (B) CD150/SLAM suckling mice were infected intranasally with either 5,000 ($n = 10$) or 10,000 ($n = 7$) PFU of MeV IC323-EGFP. (C) CD150/SLAM suckling mice were infected intranasally with 500 PFU of MeV IC323-EGFP-F L454W ($n = 5$). Cryosections of lungs (D) and brain areas (E to G) collected from CD150/SLAM suckling mice ($n = 3$) coinfected intranasally with 1,000 PFU of both MeV IC323-tdTomato and MeV IC323-EGFP-F L454W (at day 4 postinfection) were stained using anti-GFP (green) and anti-tdTomato (red) antibodies. Nuclei were counterstained with DAPI (blue). (D) Lung section. (E) Brain ventricle area (white arrows indicate the infection in meninges). (F) Cortex parenchyma. (G) Cerebellum. Scale bars, 100 μm.

previously thought and may occur in up to 1 in 600 children infected under 1 year of age (1). The third form of MeV-induced CNS disease, progressive infectious encephalitis or measles inclusion body encephalitis (MIBE), occurs in immunosuppressed patients several months after MeV infection (22, 39, 40). Acute encephalomyelitis does not seem to be associated with active viral growth in the CNS, while both SSPE and MIBE are associated with viral propagation in the CNS.

In a recent South African MeV outbreak (2014), 8 HIV-infected patients died of fatal MeV CNS manifestations (41). The F protein component of the MeV virus fusion complex recovered from the CNS of patients who suffered fatal MIBE is altered, so that F is activated in the absence of a known receptor for H (23). The usual balance maintained by F between stability of the prefusion state and activation is skewed towards activation in these isolates. The F proteins from two separate patient isolates

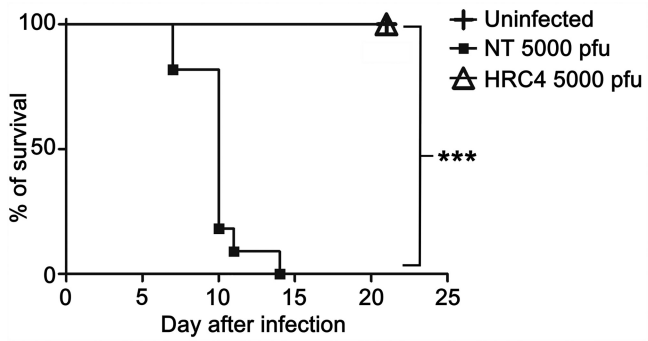

FIG 6 Fusion inhibitory peptides protect from lethal infection with virus bearing the L454W F *in vivo*. SLAM suckling mice were infected intranasally with 5,000 PFU of MeV IC323-EGFP-F L454W. A subset of animals infected with 5,000 PFU ($n = 9$) was treated with HRC4 peptide intranasally (6 mg/kg) the day before and 4 h after infection (as we have previously done for wt virus [33]). The mock-infected group received vehicle at the same time ($n = 11$). The Mantel-Cox test was used for the survival comparison analysis. ***, $P = 0.0007$.

from the outbreak contained one specific amino acid alteration at position 454 (L454W) that increased fusion even in the absence of H and markedly decreased the thermal stability of F (23). Alterations in the fusion complex have been linked to CNS adaptation and to increased neuropathogenesis (28).

MeV is a uniquely human pathogen, and none of the currently available *in vivo* models completely represent the CNS sequelae. The best current model for acute measles infection is the nonhuman primate. However, in studies in rhesus, cynomolgus, and squirrel monkeys, CNS manifestations have not been described (8, 42–48). We showed here that MeV bearing the MIBE-derived L454W F infects two animal models of MeV infection via the respiratory route. In cotton rat lungs, the mutant virus grew at even higher titers than the wt virus, indicating that L454W F may confer an advantage in this model. The lethal dose in suckling mice for L454W F bearing virus was lower than 500 PFU, in contrast to a lethal dose of around 5,000 PFU for wt virus. These two animal models suggest that the virus bearing the L454W F is pathogenic *in vivo*.

Previous experiments with MeV F proteins bearing mutations at position T461I and S103I/N462S/N465S—found in virus isolates from patients with SSPE—showed that these mutations permit the spread of virus in the CNS after intracranial inoculation in small animal models lacking known MeV receptors (28, 29). However, those viruses did not spread after intraperitoneal inoculation (29). In this study, intranasal infection of suckling SLAM transgenic mice led to viral spread in the CNS. This difference might be explained by factors, including the specific virus used, the animal model, receptor expression, and/or infection route. Our results in suckling CD150/SLAM receptor transgenic mice show that the MeV bearing F L454W can infect via the natural route of MeV infection, reach the CNS, and cause lethal disease. The wt virus in this model requires a significantly higher viral load and more time to achieve CNS infection and lethality. Host-to-host transmission was not assessed here, but the lower thermal stability of the viruses bearing the unstable F suggests that these viruses may be at a disadvantage for transmission, as they may more readily become inactivated before reaching the correct target cells. Future work will assess the pathogenicity of the L454W mutation in the context of the original B3 strain, where this mutation was initially found, with and without the additional coding and noncoding mutations found in the clinical samples (22, 23).

There are no specific therapies for acute complications of MeV or for persistent MeV CNS infections (24, 26, 49–51). For MeV cerebral infection, the only available antiviral therapy is ribavirin, which is unlikely to offer significant benefit. Ribavirin prophylaxis in a mouse model of MeV infection resulted in only 60% survival (52), in contrast with HRC4 peptide prophylaxis, which resulted in 100% survival in a similar model (34). A peptide-based prophylactic approach prevents lethal infection in CD150/SLAM trans-

genic suckling mice infected with wt MeV (33) and MeV bearing L454W F (Fig. 6). An anti-MeV strategy that combines vaccines and antivirals would contribute to better management of infected individuals and prevention and treatment of complications and could support public health objectives, including that of global eradication (53, 54).

The CNS-adapted viruses we describe are sensitive to the fusion inhibitory peptides, which act after the activation of conformational transformation in F. However, these viruses are resistant to antivirals that stabilize the prefusion state of F (35). Therapies designed to stabilize prefusion F protein are in an advanced stage of development for a related virus, respiratory syncytial virus (55). For MeV, small molecules targeting prefusion F have been identified, but resistance to these inhibitors quickly arose. For 3G—the inhibitor used in this study alongside the inhibitory peptides—resistance occurred due to a mutation at position 462 (N462K) in F, one of the mutants we analyzed here (35, 36, 56–58). The N462K F was inherently destabilized but was retained in the prefusion state in the presence of inhibitor (35, 36). FIP was reported to have a mechanism of action similar to 3G (12, 31), suggesting that MeV with L454W F may emerge under the selective pressure of a fusion inhibitor (31), and MeV bearing the L454W F was resistant to the inhibitory activity of 3G (Fig. 3 and 4; see also Fig. S1 in the supplemental material). These findings suggest that an antiviral strategy based on retaining F in its prefusion state, at least for MeV, may carry the risk of eliciting the emergence of neurotropic variant viruses.

MATERIALS AND METHODS

Ethical statement. All *in vivo* experiments with mice were performed by C. M. and C. D. (accredited by the French veterinary service) according to the French national charter on the ethics of animals, class 2, 3, and 4 genetically modified organisms (GMO) authorization number 5854. The *in vivo* protocol was also according to French ethical committee (CECCAPP) regulations, accreditation number CECCAPP_ENS_2015_011. All experiments performed in cotton rats were approved by the Institutional Animal Care and Use Committee of The Ohio State University.

Peptides and chemicals. MeV F-derived fusion inhibitory peptide HRC4 was previously described (33). Briefly, peptide dissolved in dimethyl sulfoxide (DMSO) was added to cholesterol-polyethylene glycol 4 (PEG4)-bis-maleimide dissolved in tetrahydrofuran followed by addition of *N*,*N*-diisopropylethylamine to the solution. The solution was left stirring at room temperature for 3 h and then purified by C_4 prep column (Phenomenex Jupiter C_4 liquid chromatography [LC] column, 300 Å) using as eluents 0.1% trifluoroacetic acid in water (A) and 0.1% trifluoroacetic acid in acetonitrile (B) and the following linear gradient: 30% to 80% in 20 min to 100% in 3 min, washing step at 100% for 5 min, flow 20 ml/min. The product of lyophilization was a white powder confirmed by matrix-assisted laser desorption ionization (MALDI) to be HRC4: HRC4 expected mass, 10076.4; HRC4 observed mass, 10075.4. *N*-(3-cyanophenyl)-2-phenylacetamide (also known as 3G [35, 36]) was commercially acquired from ZereneX Molecular Limited (UK). The purity of 3G was tested by high-pressure liquid chromatography (HPLC) and shown to be >95% pure.

Cells. Vero and Vero-SLAM (African green monkey kidney) (7) cells were grown in Dulbecco's modified Eagle's medium (DMEM; Invitrogen, Thermo Fisher Scientific) supplemented with 10% fetal bovine serum (FBS) and antibiotics in 5% CO_2. The 293-3-46 (59) and Vero-SLAM culture media were supplemented with Geneticin 1 mg/ml (Thermo Fisher Scientific).

Recombinant virus production and analysis. MeV IC323-EGFP (60) is a recombinant virus generated by reverse genetics using a plasmid (kindly provided by Yusuke Yanagi, Kyushu University, Fukyoka, Japan) coding for the IC323 MeV strain consensus sequence and containing an EGFP expression cassette between the leader sequence and the N viral gene.

To generate the L454W variant, the mutated F fragment was generated by PCR, inserted into the p(+)MeV_IC323-EGFP plasmid, and digested with the restriction enzymes NruI and PacI. For the MeV IC323-tdTomato plasmid, the EGFP fragment was removed from the p(+)MeV_IC323-EGFP plasmid by digestion with AscI and AatII and replaced by a PCR fragment encoding tdTomato. The PCR fragments were inserted using the In-Fusion HD Cloning kit (TaKaRa). Modified plasmids were then amplified in *Escherichia coli* Stellar bacterial cells, extracted using the NucleoBond Xtra plasmid Midiprep kit (Macherey-Nagel), and sequenced.

MeV IC323 recombinant viruses were rescued in 293-3-46 cells as previously described (59). All viruses were propagated and the titers determined in Vero-SLAM cells. Briefly, 2×10^5 293-3-46 cells were seeded in 6-well plates. The following day, cells were transfected using a ProFection mammalian transfection system, calcium phosphate kit (Promega) according to manufacturer's recommendations with 10 μg of plasmid encoding the full-length viral genome and 40 ng of pEMC-MeV-L. The next day, supernatant fluids were replaced with DMEM supplemented with 10% FBS, incubated at 42°C for 3 h, and replaced at 37°C in 5% CO_2. Three days after transfection, cells were mechanically detached by pipetting up and down and overlaid onto Vero-SLAM cells in a 10-cm culture dish. The cells were incubated for 3 to 4 days at 37°C in 5% CO_2 until the appearance of syncytia. For the production of the initial passage (i.e., P0), single syncytia were collected by scraping using a tip and pipetting in 20 μl and transferred onto

fresh Vero-SLAM cells in a well of a 6-well plate. When syncytia covered approximately 80% of the well's surface, the cells and the supernatant fluid were collected by scraping and were frozen at −80°C until use (P0 production). The passage 1 (P1) stock was made by using 300 μl of the P0 to infect a 70% confluent T150 flask of Vero-SLAM in 15 ml of Opti-MEM (2 h at 37°C). After 2 h, 15 ml of DMEM-10% FBS was added to the culture, and cells were incubated for 2 to 4 days at 32°C in 5% CO_2 until 70% to 90% infection. The virus was collected in a small volume of Opti-MEM by scraping the cells and exposed to 2 cycles of freezing and thawing at −80°C to lyse cells and detach the virus particles. Cell debris was removed by centrifugation for 10 min at 400 × g, and the viral stock in the supernatant fluid was aliquoted and kept at −80°C. After titration, the passage 2 (P2) stock was made by infecting Vero-SLAM at a multiplicity of infection (MOI) of 0.03 using the P1 viral stock and collected the same way as for the P1.

Structural modeling. Twenty models were produced for the wild-type (wt) measles virus fusion glycoprotein (MeV F) using the protein homology server Phyre2 (61) based on the postfusion structure of hPIV3-F as a template (PDB ID 1ZTM) (62). The resulting models were subsequently optimized via Dunbrack rotamer library and the REF15 scoring function through the PyRosetta (63, 64), resulting in a model for the conformation of the postfusion MeV-F. The crystal structure is represented for the prefusion MeV-F (PDB ID 5YXW) (12). All structural figures were produced using PyMol (http://www.pymol.org/).

Infectivity of MeV variants. Aliquots of equal volumes of DMEM containing 1,000 PFU of virus (MeV IC323-EGFP, MeV IC323-EGFP-F L454W, MeV IC323-EGFP-F T461I, and MeV IC323-EGFP-F N462K) were incubated at a range of temperatures from 4 to 55°C for 5 to 30 min. The titers from samples were then determined on Vero-SLAM cells in triplicates. Results are presented as means ± standard deviations from 3 separate experiments.

***β*-Gal complementation-based fusion assay.** To quantify cell-to-cell fusion, we used a fusion assay based on alpha-omega complementation of β-galactosidase (β-Gal) that was previously described (37, 65). Briefly, 293T cells transiently transfected with the omega reporter subunit and the receptor plasmids were incubated with cells coexpressing viral glycoproteins and the alpha reporter subunit in the presence or absence of MeV F HRC4 dimeric fusion inhibitory peptide or 3G. Cell fusion, which leads to β-Gal complementation, was stopped by lysing the cells, and the luminescence after adding the Galacton-Star substrate (Applied Biosystems) was measured on an Infinite M1000 Pro (Tecan) microplate reader.

Plaque enlargement assay. Vero or Vero-SLAM cells were plated in 12-well plates (2×10^5 cells/well). The following day, cells were infected either with MeV IC323-EGFP or with MeV IC323-EGFP-F L454W (100 PFU/well for Vero-SLAM and 500 PFU/well for Vero cells) for 2 h at 32°C. The medium was replaced with medium containing 2% of methylcellulose Avicel/2× complete medium (1:1) and serial dilutions of either *N*-(3-cyanophenyl)-2-phenylacetamide, referred to as 3G (35), or MeV F-derived HRC4 dimeric fusion inhibitory peptide (33, 34). After 24 h, 48 h, or 72 h, medium was removed, cells were rinsed with phosphate-buffered saline (PBS), and pictures were obtained on a ZOE Fluorescent cell imager (Bio-Rad). Areas of infection in pixels were measured using ImageJ software on images randomly acquired from separated experiments ($n = 3$ at least; analyzed by two-way ANOVA).

***In vivo* experiments. (i) Mice.** One-week-old SLAM transgenic (tg) mice, highly susceptible to MeV infection (33, 38), were infected intranasally (i.n.) by inoculation of 5 μl of Opti-MEM (Thermo Fisher Scientific) containing either 500 or 5,000 PFU of MeV IC323-EGFP-F L454W. Infection with MeV IC323-EGFP F wt was performed with 5,000 or 10,000 PFU. Animals were treated with HRC4 i.n. (6 mg/kg) 24 h before and 4 h after infection (5 μl of peptide). Mock groups received vehicle (Milli-Q water containing 10% DMSO). All animals were observed daily for 21 days, and those showing clinical signs, including neurological symptoms, ataxia, or lethargy, were euthanized. SLAM tg mice (male and female, bred at the Institute's animal facility, PBES, ENS-Lyon) were handled in strict accordance with good animal practice as defined by the French National Charter on the Ethics of Animal Experimentation.

(ii) Cotton rats. Inbred cotton rats (*Sigmodon hispidus*) were purchased from Envigo, Inc., Indianapolis. Both male and female cotton rats aged 5 to 7 weeks were used. For i.n. infection, 10^5 $TCID_{50}$ of MeV IC323-EGFP F wt or MeV IC323-EGFP-F L454W in PBS was inoculated intranasally to isoflurane-anesthetized cotton rats in a volume of 100 μl. Four days after infection, the animals were euthanized by CO_2 inhalation, and their lungs were collected and weighed. Lung tissue was minced with scissors and homogenized with a glass dounce homogenizer. Serial 10-fold dilutions of supernatant fluids were assessed for the presence of infectious virus in 48-well plates using cytopathic effect (CPE) in Vero SLAM cells as the endpoint. Plates were scored for CPE microscopically after 7 days. The $TCID_{50}$ was calculated as described previously (33).

Coinfection and immunofluorescence. One-week-old SLAM tg mice ($n = 3$) received 1,000 PFU of both MeV IC323-tdTomato F wt and MeV IC323-EGFP-F L454W intranasally in 5 μl of Opti-MEM. After 4 days, the animals were euthanized by cervical dislocation, and the brains and lungs were collected. Organs were fixed overnight in 4% paraformaldehyde (PFA), washed in 1× Dulbecco's phosphate-buffered saline (DPBS), placed in 30% sucrose, and frozen in cold isopentane on dry ice. Cryosections (7-μm thick) were dried for 30 min at room temperature (RT) and permeabilized and blocked in 1× DPBS-4% FBS-0.3% Triton X-100 for 20 min at RT. Sections were incubated in 1× DPBS-4% FBS-0.3% Triton X-100 containing mouse anti-GFP (catalog number AB1218; Abcam) (1:500) and goat anti-tdTomato (catalog number AB8181-200; Sicgen antibodies) (1:500) for 1 h at RT. After 3 washes (5 min each) in 1× DPBS, tissue sections were incubated in 1× DPBS-4% FBS-0.3% Triton X-100 containing the secondary donkey anti-rabbit conjugated with Alexa 488 and donkey anti-goat conjugated with Alexa

555 antibodies (1:500 each) for 1 h at RT. Nuclei were counterstained with DAPI (4′,6-diamidino-2-phenylindole).

Statistical analysis. The Mantel-Cox test was used for the survival comparison analysis. The two-way ANOVA with Bonferroni's posttest was used to compare the thermal stability of the different viruses and to compare plaque enlargement in the presence or absence of receptor and/or antiviral compound. All other statistical comparisons were performed using the Mann-Whitney U test. All analyses were performed with GraphPad Prism 5 software.

SUPPLEMENTAL MATERIAL

Supplemental material for this article may be found at https://doi.org/10.1128/JVI.01862-18.

SUPPLEMENTAL FILE 1, PDF file, 0.4 MB.

ACKNOWLEDGMENTS

The work was supported by NIH AI121349, NS091263, and NS105699 to M.P., by French ANR NITRODEP (ANR-13-PDOC-0010-01) to C.M., by Region Auvergne Rhone Alpes and LABEX ECOFECT (ANR-11-LABX-0048) of Lyon University, within the program "Investissements d'Avenir" (ANR-11-IDEX-0007) operated by the French National Research Agency (ANR), to B.H., and by Japan AMED J-PRIDE (JP18fm0208022h) to T.H.

REFERENCES

1. Moss WJ, Griffin DE. 2012. Measles. Lancet 379:153–164. https://doi.org/10.1016/S0140-6736(10)62352-5.
2. Perry RT, Murray JS, Gacic-Dobo M, Dabbagh A, Mulders MN, Strebel PM, Okwo-Bele J-M, Rota PA, Goodson JL. 2015. Progress toward regional measles elimination - worldwide, 2000–2014. MMWR Morb Mortal Wkly Rep 64:1246–1251.
3. Simons E, Ferrari M, Fricks J, Wannemuehler K, Anand A, Burton A, Strebel P. 2012. Assessment of the 2010 global measles mortality reduction goal: results from a model of surveillance data. Lancet 379:2173–2178. https://doi.org/10.1016/S0140-6736(12)60522-4.
4. Niewiesk S. 2014. Maternal antibodies: clinical significance, mechanism of interference with immune responses, and possible vaccination strategies. Front Immunol 5:446. https://doi.org/10.3389/fimmu.2014.00446.
5. Jansen VA, Stollenwerk N, Jensen HJ, Ramsay ME, Edmunds WJ, Rhodes CJ. 2003. Measles outbreaks in a population with declining vaccine uptake. Science 301:804. https://doi.org/10.1126/science.1086726.
6. Melenotte C, Zandotti C, Gautret P, Parola P, Raoult D. 2018. Measles: is a new vaccine approach needed? Lancet Infect Dis 18:1060–1061. https://doi.org/10.1016/S1473-3099(18)30543-7.
7. Tatsuo H, Ono N, Tanaka K, Yanagi Y. 2000. SLAM (CDw150) is a cellular receptor for measles virus. Nature 406:893–897. https://doi.org/10.1038/35022579.
8. Mühlebach MD, Mateo M, Sinn PL, Prüfer S, Uhlig KM, Leonard VHJ, Navaratnarajah CK, Frenzke M, Wong XX, Sawatsky B, Ramachandran S, McCray PB, Cichutek K, von Messling V, Lopez M, Cattaneo R. 2011. Adherens junction protein nectin-4 is the epithelial receptor for measles virus. Nature 480:530–533. https://doi.org/10.1038/nature10639.
9. Noyce RS, Bondre DG, Ha MN, Lin L-T, Sisson G, Tsao M-S, Richardson CD. 2011. Tumor cell marker PVRL4 (nectin 4) is an epithelial cell receptor for measles virus. PLoS Pathog 7:e1002240. https://doi.org/10.1371/journal.ppat.1002240.
10. Chang A, Dutch RE. 2012. Paramyxovirus fusion and entry: multiple paths to a common end. Viruses 4:613–636. https://doi.org/10.3390/v4040613.
11. Harrison SC. 2008. Viral membrane fusion. Nat Struct Mol Biol 15:690–698. https://doi.org/10.1038/nsmb.1456.
12. Hashiguchi T, Fukuda Y, Matsuoka R, Kuroda D, Kubota M, Shirogane Y, Watanabe S, Tsumoto K, Kohda D, Plemper RK, Yanagi Y. 2018. Structures of the prefusion form of measles virus fusion protein in complex with inhibitors. Proc Natl Acad Sci U S A 115:2496–2501. https://doi.org/10.1073/pnas.1718957115.
13. Lambert DM, Barney S, Lambert AL, Guthrie K, Medinas R, Davis DE, Bucy T, Erickson J, Merutka G, Petteway SR. 1996. Peptides from conserved regions of paramyxovirus fusion (F) proteins are potent inhibitors of viral fusion. Proc Natl Acad Sci U S A 93:2186–2191. https://doi.org/10.1073/pnas.93.5.2186.
14. Allen IV, McQuaid S, McMahon J, Kirk J, McConnell R. 1996. The significance of measles virus antigen and genome distribution in the CNS in SSPE for mechanisms of viral spread and demyelination. J Neuropathol Exp Neurol 55:471–480. https://doi.org/10.1097/00005072-199604000-00010.
15. Buchanan R, Bonthius DJ. 2012. Measles virus and associated central nervous system sequelae. Semin Pediatr Neurol 19:107–114. https://doi.org/10.1016/j.spen.2012.02.003.
16. Hosoya M. 2006. Measles encephalitis: direct viral invasion or autoimmune-mediated inflammation? Intern Med 45:841–842. https://doi.org/10.2169/internalmedicine.45.0161.
17. Cattaneo R, Schmid A, Billeter MA, Sheppard RD, Udem SA. 1988. Multiple viral mutations rather than host factors cause defective measles virus gene expression in a subacute sclerosing panencephalitis cell line. J Virol 62:1388–1397.
18. Rima BK, Duprex WP. 2005. Molecular mechanisms of measles virus persistence. Virus Res 111:132–147. https://doi.org/10.1016/j.virusres.2005.04.005.
19. Schmid A, Spielhofer P, Cattaneo R, Baczko K, ter Meulen V, Billeter MA. 1992. Subacute sclerosing panencephalitis is typically characterized by alterations in the fusion protein cytoplasmic domain of the persisting measles virus. Virology 188:910–915. https://doi.org/10.1016/0042-6822(92)90552-Z.
20. Baldolli A, Dargère S, Cardineau E, Vabret A, Dina J, de La Blanchardière A, Verdon R. 2016. Measles inclusion-body encephalitis (MIBE) in a immunocompromised patient. J Clin Virol 81:43–46. https://doi.org/10.1016/j.jcv.2016.05.016.
21. Hughes I, Jenney ME, Newton RW, Morris DJ, Klapper PE. 1993. Measles encephalitis during immunosuppressive treatment for acute lymphoblastic leukaemia. Arch Dis Child 68:775–778. https://doi.org/10.1136/adc.68.6.775.
22. Hardie DR, Albertyn C, Heckmann JM, Smuts HEM. 2013. Molecular characterisation of virus in the brains of patients with measles inclusion body encephalitis (MIBE). Virol J 10:283. https://doi.org/10.1186/1743-422X-10-283.
23. Jurgens EM, Mathieu C, Palermo LM, Hardie D, Horvat B, Moscona A, Porotto M. 2015. Measles fusion machinery is dysregulated in neuropathogenic variants. mBio 6:e02528-14. https://doi.org/10.1128/mBio.02528-14.
24. Makhortova NR, Askovich P, Patterson CE, Gechman LA, Gerard NP, Rall GF. 2007. Neurokinin-1 enables measles virus trans-synaptic spread in neurons. Virology 362:235–244. https://doi.org/10.1016/j.virol.2007.02.033.
25. Watanabe M, Hashimoto K, Abe Y, Kodama EN, Nabika R, Oishi S, Ohara S, Sato M, Kawasaki Y, Fujii N, Hosoya M. 2016. A novel peptide derived from the fusion protein heptad repeat inhibits replication of subacute sclerosing panencephalitis virus *in vitro* and *in vivo*. PLoS One 11:e0162823. https://doi.org/10.1371/journal.pone.0162823.

26. Young VA, Rall GF. 2009. Making it to the synapse: measles virus spread in and among neurons. Curr Top Microbiol Immunol 330:3–30.
27. Ayata M, Takeuchi K, Takeda M, Ohgimoto S, Kato S, Sharma LB, Tanaka M, Kuwamura M, Ishida H, Ogura H. 2010. The F gene of the Osaka-2 strain of measles virus derived from a case of subacute sclerosing panencephalitis is a major determinant of neurovirulence. J Virol 84:11189–11199. https://doi.org/10.1128/JVI.01075-10.
28. Watanabe S, Shirogane Y, Suzuki SO, Ikegame S, Koga R, Yanagi Y. 2013. Mutant fusion proteins with enhanced fusion activity promote measles virus spread in human neuronal cells and brains of suckling hamsters. J Virol 87:2648–2659. https://doi.org/10.1128/JVI.02632-12.
29. Watanabe S, Ohno S, Shirogane Y, Suzuki SO, Koga R, Yanagi Y. 2015. Measles virus mutants possessing the fusion protein with enhanced fusion activity spread effectively in neuronal cells, but not in other cells, without causing strong cytopathology. J Virol 89:2710–2717. https://doi.org/10.1128/JVI.03346-14.
30. Sato Y, Watanabe S, Fukuda Y, Hashiguchi T, Yanagi Y, Ohno S. 2018. Cell-to-cell measles virus spread between human neurons is dependent on hemagglutinin and hyperfusogenic fusion protein. J Virol 92:e02166-17. https://doi.org/10.1128/JVI.02166-17.
31. Ha MN, Delpeut S, Noyce RS, Sisson G, Black KM, Lin L-T, Bilimoria D, Plemper RK, Privé GG, Richardson CD. 2017. Mutations in the fusion protein of measles virus that confer resistance to the membrane fusion inhibitors carbobenzoxy-D-Phe-L-Phe-Gly and 4-nitro-2-phenylacetyl amino-benzamide. J Virol 91:e01026-17. https://doi.org/10.1128/JVI.01026-17.
32. Yin H-S, Paterson RG, Wen X, Lamb RA, Jardetzky TS. 2005. Structure of the uncleaved ectodomain of the paramyxovirus (hPIV3) fusion protein. Proc Natl Acad Sci U S A 102:9288–9293. https://doi.org/10.1073/pnas.0503989102.
33. Mathieu C, Huey D, Jurgens E, Welsch JC, DeVito I, Talekar A, Horvat B, Niewiesk S, Moscona A, Porotto M. 2015. Prevention of measles virus infection by intranasal delivery of fusion inhibitor peptides. J Virol 89:1143–1155. https://doi.org/10.1128/JVI.02417-14.
34. Welsch JC, Talekar A, Mathieu C, Pessi A, Moscona A, Horvat B, Porotto M. 2013. Fatal measles virus infection prevented by brain-penetrant fusion inhibitors. J Virol 87:13785–13794. https://doi.org/10.1128/JVI.02436-13.
35. Avila M, Alves L, Khosravi M, Ader-Ebert N, Origgi F, Schneider-Schaulies J, Zurbriggen A, Plemper RK, Plattet P. 2014. Molecular determinants defining the triggering range of prefusion F complexes of canine distemper virus. J Virol 88:2951–2966. https://doi.org/10.1128/JVI.03123-13.
36. Ader N, Brindley M, Avila M, Örvell C, Horvat B, Hiltensperger G, Schneider-Schaulies J, Vandevelde M, Zurbriggen A, Plemper RK, Plattet P. 2013. Mechanism for active membrane fusion triggering by morbillivirus attachment protein. J Virol 87:314–326. https://doi.org/10.1128/JVI.01826-12.
37. Porotto M, Fornabaio M, Kellogg GE, Moscona A. 2007. A second receptor binding site on human parainfluenza virus type 3 hemagglutinin-neuraminidase contributes to activation of the fusion mechanism. J Virol 81:3216–3228. https://doi.org/10.1128/JVI.02617-06.
38. Sellin CI, Davoust N, Guillaume V, Baas D, Belin M-F, Buckland R, Wild TF, Horvat B. 2006. High pathogenicity of wild-type measles virus infection in CD150 (SLAM) transgenic mice. J Virol 80:6420–6429. https://doi.org/10.1128/JVI.00209-06.
39. Fox A, Hung TM, Wertheim H, Hoa LNM, Vincent A, Lang B, Waters P, Ha NH, Trung NV, Farrar J, Van Kinh N, Horby P. 2013. Acute measles encephalitis in partially vaccinated adults. PLoS One 8:e71671. https://doi.org/10.1371/journal.pone.0071671.
40. Mahil SK, Fleming J, Robson A, Sarkany R. 2014. Measles in a previously vaccinated human immunodeficiency virus-positive adult. Clin Exp Dermatol 39:117–118. https://doi.org/10.1111/ced.12238.
41. Albertyn C, van der Plas H, Hardie D, Candy S, Tomoka T, Leepan EB, Heckmann JM. 2011. Silent casualties from the measles outbreak in South Africa. S Afr Med J 101:313–317. https://doi.org/10.7196/SAMJ.4616.
42. Devaux P, Hodge G, McChesney MB, Cattaneo R. 2008. Attenuation of V- or C-defective measles viruses: infection control by the inflammatory and interferon responses of rhesus monkeys. J Virol 82:5359–5367. https://doi.org/10.1128/JVI.00169-08.
43. Frenzke M, Sawatsky B, Wong XX, Delpeut S, Mateo M, Cattaneo R, von Messling V. 2013. Nectin-4-dependent measles virus spread to the cynomolgus monkey tracheal epithelium: role of infected immune cells infiltrating the lamina propria. J Virol 87:2526–2534. https://doi.org/10.1128/JVI.03037-12.
44. Lemon K, de Vries RD, Mesman AW, McQuaid S, van Amerongen G, Yüksel S, Ludlow M, Rennick LJ, Kuiken T, Rima BK, Geijtenbeek TBH, Osterhaus ADME, Duprex WP, de Swart RL. 2011. Early target cells of measles virus after aerosol infection of non-human primates. PLoS Pathog 7:e1001263. https://doi.org/10.1371/journal.ppat.1001263.
45. Leonard VHJ, Sinn PL, Hodge G, Miest T, Devaux P, Oezguen N, Braun W, McCray PB, McChesney MB, Cattaneo R. 2008. Measles virus blind to its epithelial cell receptor remains virulent in rhesus monkeys but cannot cross the airway epithelium and is not shed. J Clin Invest 118:2448–2458. https://doi.org/10.1172/JCI35454.
46. Leonard VHJ, Hodge G, Reyes-Del Valle J, McChesney MB, Cattaneo R. 2010. Measles virus selectively blind to signaling lymphocytic activation molecule (SLAM; CD150) is attenuated and induces strong adaptive immune responses in rhesus monkeys. J Virol 84:3413–3420. https://doi.org/10.1128/JVI.02304-09.
47. Delpeut S, Sawatsky B, Wong X-X, Frenzke M, Cattaneo R, von Messling V. 2017. Nectin-4 interactions govern measles virus virulence in a new model of pathogenesis, the squirrel monkey (*Saimiri sciureus*). J Virol 91:e02490-16. https://doi.org/10.1128/JVI.02490-16.
48. Devaux P, Hudacek AW, Hodge G, Reyes-del Valle J, McChesney MB, Cattaneo R. 2011. A recombinant measles virus unable to antagonize STAT1 function cannot control inflammation and is attenuated in rhesus monkeys. J Virol 85:348–356. https://doi.org/10.1128/JVI.00802-10.
49. Chiu MH, Meatherall B, Nikolic A, Cannon K, Fonseca K, Joseph JT, MacDonald J, Pabbaraju K, Tellier R, Wong S, Koch MW. 2016. Subacute sclerosing panencephalitis in pregnancy. Lancet Infect Dis 16:366–375. https://doi.org/10.1016/S1473-3099(15)00524-1.
50. O'Donnell LA, Rall GF. 2010. Blue moon neurovirology: the merits of studying rare CNS diseases of viral origin. J Neuroimmune Pharmacol 5:443–455. https://doi.org/10.1007/s11481-010-9200-4.
51. Reuter D, Schneider-Schaulies J. 2010. Measles virus infection of the CNS: human disease, animal models, and approaches to therapy. Med Microbiol Immunol 199:261–271. https://doi.org/10.1007/s00430-010-0153-2.
52. Jeulin H, Venard V, Carapito D, Finance C, Kedzierewicz F. 2009. Effective ribavirin concentration in mice brain using cyclodextrin as a drug carrier: evaluation in a measles encephalitis model. Antiviral Res 81:261–266. https://doi.org/10.1016/j.antiviral.2008.12.006.
53. Plemper RK, Hammond AL. 2014. Synergizing vaccinations with therapeutics for measles eradication. Expert Opin Drug Discov 9:201–214. https://doi.org/10.1517/17460441.2014.867324.
54. Plemper RK, Snyder JP. 2009. Measles control–can measles virus inhibitors make a difference? Curr Opin Investig Drugs 10:811–820.
55. Battles MB, Langedijk JP, Furmanova-Hollenstein P, Chaiwatpongsakorn S, Costello HM, Kwanten L, Vranckx L, Vink P, Jaensch S, Jonckers THM, Koul A, Arnoult E, Peeples ME, Roymans D, McLellan JS. 2016. Molecular mechanism of respiratory syncytial virus fusion inhibitors. Nat Chem Biol 12:87–93. https://doi.org/10.1038/nchembio.1982.
56. Plemper RK, Doyle J, Sun A, Prussia A, Cheng L-T, Rota PA, Liotta DC, Snyder JP, Compans RW. 2005. Design of a small-molecule entry inhibitor with activity against primary measles virus strains. Antimicrob Agents Chemother 49:3755–3761. https://doi.org/10.1128/AAC.49.9.3755-3761.2005.
57. Prussia AJ, Plemper RK, Snyder JP. 2008. Measles virus entry inhibitors: a structural proposal for mechanism of action and the development of resistance. Biochemistry 47:13573–13583. https://doi.org/10.1021/bi801513p.
58. Sun A, Prussia A, Zhan W, Murray EE, Doyle J, Cheng L-T, Yoon J-J, Radchenko EV, Palyulin VA, Compans RW, Liotta DC, Plemper RK, Snyder JP. 2006. Nonpeptide inhibitors of measles virus entry. J Med Chem 49:5080–5092. https://doi.org/10.1021/jm0602559.
59. Radecke F, Spielhofer P, Schneider H, Kaelin K, Huber M, Dötsch C, Christiansen G, Billeter MA. 1995. Rescue of measles viruses from cloned DNA. EMBO J 14:5773–5784. https://doi.org/10.1002/j.1460-2075.1995.tb00266.x.
60. Hashimoto K, Ono N, Tatsuo H, Minagawa H, Takeda M, Takeuchi K, Yanagi Y. 2002. SLAM (CD150)-independent measles virus entry as revealed by recombinant virus expressing green fluorescent protein. J Virol 76:6743–6749. https://doi.org/10.1128/JVI.76.13.6743-6749.2002.
61. Kelley LA, Mezulis S, Yates CM, Wass MN, Sternberg MJE. 2015. The

Phyre2 web portal for protein modeling, prediction and analysis. Nat Protoc 10:845–858. https://doi.org/10.1038/nprot.2015.053.
62. McRee DE. 1999. XtalView/Xfit–A versatile program for manipulating atomic coordinates and electron density. J Struct Biol 125:156–165. https://doi.org/10.1006/jsbi.1999.4094.
63. Alford RF, Leaver-Fay A, Jeliazkov JR, O'Meara MJ, DiMaio FP, Park H, Shapovalov MV, Renfrew PD, Mulligan VK, Kappel K, Labonte JW, Pacella MS, Bonneau R, Bradley P, Dunbrack RL, Das R, Baker D, Kuhlman B, Kortemme T, Gray JJ. 2017. The Rosetta all-atom energy function for macromolecular modeling and design. J Chem Theory Comput 13:3031–3048. https://doi.org/10.1021/acs.jctc.7b00125.
64. Roberts E, Eargle J, Wright D, Luthey-Schulten Z. 2006. MultiSeq: unifying sequence and structure data for evolutionary analysis. BMC Bioinformatics 7:382. https://doi.org/10.1186/1471-2105-7-382.
65. Moosmann P, Rusconi S. 1996. Alpha complementation of LacZ in mammalian cells. Nucleic Acids Res 24:1171–1172. https://doi.org/10.1093/nar/24.6.1171.